双温工艺瞬时液相扩散连接 45MnMoB 地质钻杆

王学刚， 严 黔， 李辛庚
（山东电力高等专科学校 特种焊接与新材料实验室，济南 250002）

王学刚

摘 要：采用瞬时液相扩散连接技术进行了 45MnMoB 地质钻杆焊接试验，探讨了两种焊接工艺下接头的组织和力学性能。结果表明，在两种焊接工艺下，焊缝区晶粒已实现跨界面连续生长，焊缝区组织与母材组织相同，都为回火索氏体。与传统单温焊接工艺相比，1 250～1 230 ℃双温焊接工艺获得的接头无异质界面、焊合率高，接头抗拉强度为 890 MPa，弯曲 180° 不裂，达到了地质钻杆焊接接头技术要求。另外，采用瞬时液相扩散连接工艺获得的地质钻杆接头成形好，焊后无需机械加工，降低了钻杆的制造成本。

关键词：地质钻杆；45MnMoB；瞬时液相扩散连接；双温工艺；力学性能
中图分类号：TG456.9 文献标识码：A 文章编号：0253－360X(2007)05－053－04

0 序 言

国内岩心钻探钻杆是在杆体两端用螺纹连接两个公母接头，这样即使螺纹设计合理，但杆体螺纹与其母材相比强度降低一倍，往往折断事故就发生在此处。采用等离子弧焊或者摩擦焊，在杆体两端各焊接一个加厚的公母接头成为钻杆生产的一个新的结构形式。等离子弧焊在钻杆焊接中内表面余高大，且有焊瘤，必须用机械方法消除；引弧和收弧处焊缝内的气孔较难清除；一个接头需要焊三次才能完成，因此在生产中有一定的局限性。摩擦焊接头中很难避免“灰斑”缺陷，接头内外表面有飞边，需用机械加工方法清除；而当钻杆较长，接头距端部较远时，飞边很难清除，这就限制了摩擦焊在地质钻杆中的应用。周大中等人[1] 在进行 45MnMoB 地质钻杆焊接时，提出了钻杆外等离子弧焊(PAW)和钻杆孔内钨极氩弧焊(TIG)同时进行的 PAW－TIG 联焊方法。该种焊接工艺生产的钻杆不必进行焊接接头的机械加工就能直接投入使用，焊接接头经 620～640 ℃，10 min 回火处理，抗拉强度为 730～815 MPa，冷弯试验面弯角 90° 不裂。但是该工艺焊前准备工作多、操作复杂、参数精度要求严格。

瞬时液相(transient liquid phase，简称 TLP)扩散连接是将中间层合金置于装配好的工件之间，并施加一定的压力，然后加热到连接温度。在连接温度下保温时，依靠中间层与母材间的元素扩散导致接头发生等温凝固，并随后发生均匀化，形成与母材组织、成分、性能相同的接头[2]。传统的 TLP 连接工艺，通过一次保温过程就可以实现母材的连接。文献[3] 在开发 T91 耐热钢的瞬时液相扩散连接工艺过程中，提出了一种新的连接工艺模型—双温工艺模型：等温凝固以前先进行短时高温加热，然后再降到连接温度进行等温凝固和均匀化。

文中采用单温焊接工艺和双温焊接工艺进行 45MnMoB 地质钻杆的瞬时液相扩散连接，研究了两种焊接工艺下接头的性能和组织。

1 试 验

试验材料的规格为 φ71 mm×5 mm 的 45MnMoB 地质钻杆，中间层合金为自主研制的铁基非晶箔带[4]，其化学成分(质量分数，%)为：Fe 56，Ni 33，Cr 3，Si 5，B 3，熔点为 1 090～1 120 ℃，箔带厚度为 60 μm。

焊接试验参照文献[5] 进行，焊接工艺参数见表 1。焊后对焊接接头进行 650 ℃，5 min 的回火处理，以消除焊接应力、改善组织、提高性能。依照国家标准 GB2651－89《焊接接头拉伸试验方法》和国家标准 GB2653－89《焊接接头弯曲及压扁试验方法》，进行室温拉伸和弯曲试验。采用扫描电镜(SEM)和电子探针(EPMA)观察接头组织以及分析接头区合金元素的分布情况。

收稿日期：2006－06－26
基金项目：国家科技成果重点推广计划资助项目(2005EC000213)

表 1 TLP 连接工艺参数

Table 1 Parameters of TLP bonding

试样	温度 T/℃		时间 t/min		压力 p/MPa
	T_1	T_2	t_1	t_2	
1	1 250	1 250	1	1	9
2	1 230	1 230	1	2	9
3	1 250	1 230	1	2	9

2 试验结果与分析

2.1 接头性能

图 1 为地质钻杆 TLP 连接后的接头形貌。可以看出，采用 TLP 连接技术获得的焊缝内外表面无余高、成形光滑平整、无摩擦焊时的飞边和等离子焊的焊瘤、无需机械加工即可直接使用。

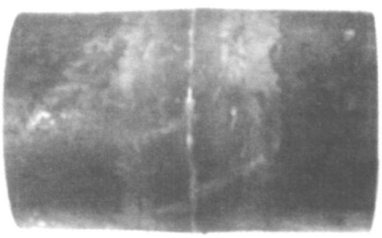

图 1 地质钻杆 TLP 连接焊缝的宏观形貌

Fig. 1 TLP bonded joint of geological drill pipe

不同焊接工艺下获得接头的力学性能如表 2 所示。表中还列出了钻杆焊接接头技术要求[1]。由表可以看出，1 230 ℃单温焊接工艺获得接头抗拉强度低于 1 250 ℃单温焊接工艺，但两者的接头塑性都很差；1 250～1 230 ℃双温焊接工艺获得的接头抗拉强度、弯曲性能均高于单温焊接工艺，并且达到钻杆焊接接头的技术要求。与 PAW－TIG 联焊工艺相比，TLP 连接工艺可获得更高质量的接头。

表 2 接头力学性能及技术要求

Table 2 Mechanical properties of TLP bonded joints and specification of geological drill pipe

试样	抗拉强度 R_m/MPa	弯曲角 θ(°)
1	880	0
2	785	0
3	890	180
钻杆焊接技术要求	＞700	≥90

2.2 接头组织

图 2 为采用不同工艺焊接 45MnMoB 钻杆的接头组织。可以看出，在两种焊接工艺下，焊缝区晶粒已实现跨界面连续生长，焊缝区组织与母材组织相同，都为回火索氏体，因此焊缝具有较高的强度。但在不同的焊接工艺下，焊缝处产生了不同的缺陷（图中箭头所示），1 250 ℃焊接接头组织中出现了树枝状的异质相，1 230 ℃焊接接头组织中出现了颗粒状异质相，而 1 250～1 230 ℃焊接接头中无异质相生成，接头仅有少量的细小空洞。另外，1 250 ℃焊接组织比 1 230 ℃焊接组织细小，这说明在 1 230～1 250 ℃之间进行 45MnMoB 焊接，焊缝晶粒长大主要受时间影响。

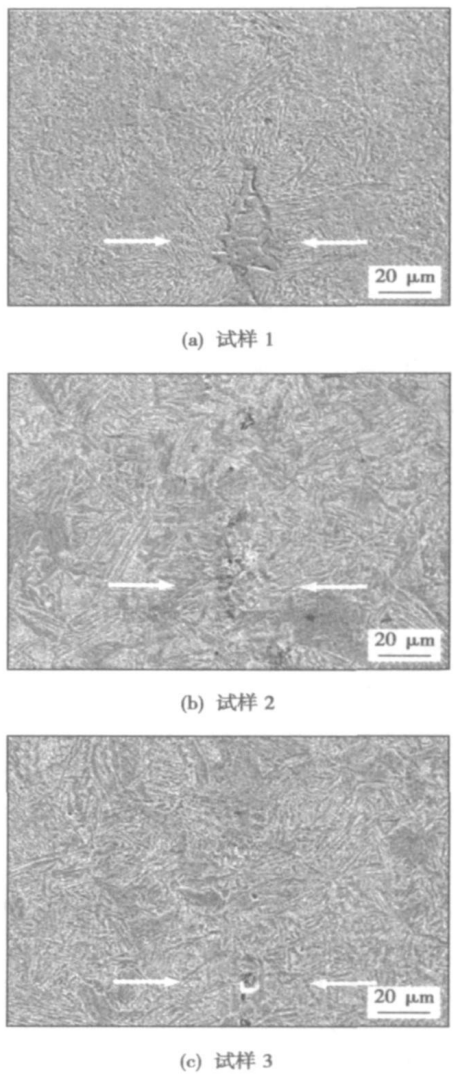

图 2 45MnMoB 钻杆瞬时液相扩散焊组织

Fig. 2 Microstructures of 45MnMoB drill pipe joint by TLP bonding

图 3 为两种工艺接头区域成分分布的 EPMA 分析结果（图 2 箭头所示位置）。两种工艺下，基体 Fe 元素在接头区均匀分布。1 250 ℃单温工艺，异质相

中Mo, B 元素的含量远远高于两侧母材，Si 元素的含量稍高于两侧母材。1 230 ℃单温工艺，异质相中 Ni, Si 元素含量出现了波峰，而 Mo, B 元素含量基本均匀分布。双温焊接工艺下焊缝中 Ni, Si 元素含量稍高，但未出现明显的波峰，空洞内有少量 CO_2 反应型气孔。

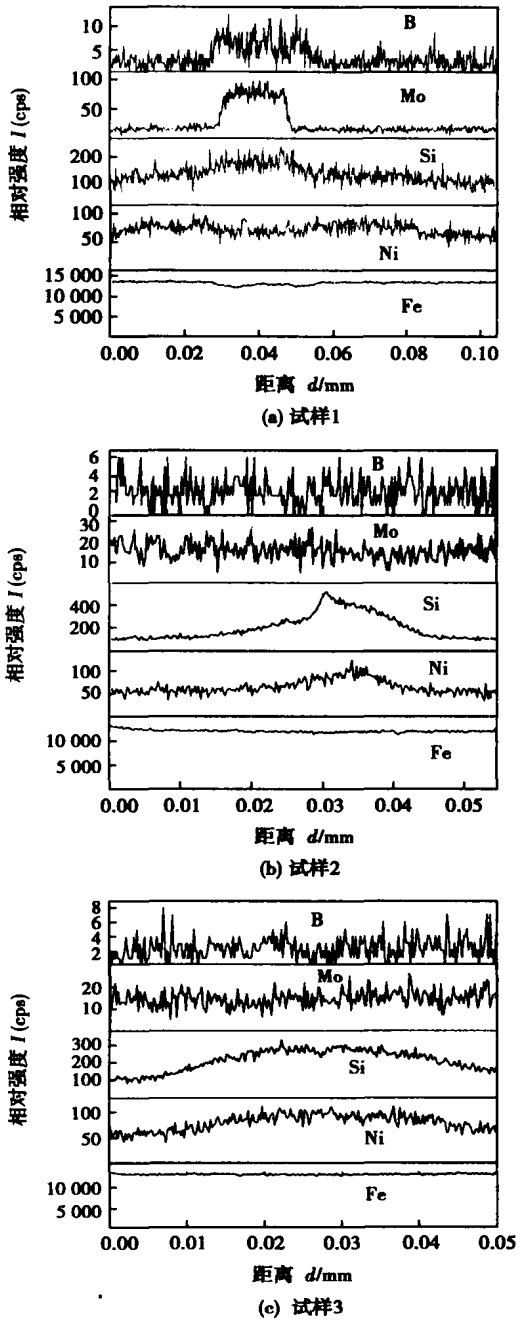

图 3　接头区域合金元素成分 EPMA 分析

Fig. 3　Element distribution in TLP bonded joint

在文中试验条件下，由于焊缝处存在缺陷（异质相和空洞），降低了焊缝的焊合率，焊缝强度低于母材强度。由于保温时间短，晶粒未长大，因此 1 250 ℃焊接接头的抗拉强度高于 1 230 ℃焊接接头强度。单温焊接工艺焊缝区的粗大异质相成为焊缝失效的裂纹源，故焊缝塑性差；而双温焊接工艺无异质相生成，仅有少量的细小空洞，因此焊缝塑性高。

3　讨　　论

文献[3] 认为，TLP 连接中采用双温焊接工艺，利用短时高温和连接温度之间的过冷度使液相发生不平衡结晶，改变了液固界面，消除了平衡结晶产生的平直连接界面。作者在进行 45MnMoB 钻杆的 TLP 连接时却得出了与文献[3] 不同的试验结果。两种焊接工艺获得的焊缝区都不存在连接界面，焊缝组织与母材组织相同，但是单温焊接工艺存在异质相，双温焊接工艺无异质相。研究表明[6,7]，以铝作中间层进行铝合金的 TLP 连接，获得了非平面界面。以铜作中间层，采用温度梯度 TLP 连接工艺也可获得非平面界面。这说明中间层和加热方式均对界面形貌产生影响。文中双温工艺主要是影响元素扩散，降低异质相的形成和存在形式。

在钢的 TLP 连接中，由于降熔元素（B, Si）的扩散使液固界面区的成分和熔点发生变化，从而发生等温凝固而实现冶金接合。从 B/Fe, B/Ni 二元相图看[8]，室温下 B 元素在 Fe, Ni 中的溶解度几乎为零，过量的 B 元素将以化合物形式存在而影响了接头性能。因此，保证降熔元素充分扩散至母材，使其在接头区的含量降至足够低，才能降低化合物相的不利影响。研究表明，对碳钢而言，焊接加热过程中铁素体—奥氏体的组织转变时间极短，只要加热稍超过 Ac_3 点，母材基本上全部为奥氏体。因此，两种焊接工艺下，45MnMoB 钻杆连接时的组织都为奥氏体，其对合金元素的扩散作用是相同的。由扩散定律可知，影响元素扩散的主要因素就是连接温度。与 1 230 ℃单温工艺相比，1 250 ℃单温工艺下，合金元素的扩散速度快。由于降熔元素 B, Si 向母材的扩散距离较远，在连接界面处形成的较宽的瞬时液相，母材在液相中间层内溶解充分，母材元素 Mo 也大量向中间层扩散。在随后的冷却过程中，母材表面破碎的氧化膜成为异质相形核点，故在焊缝处会出现富集 Mo 的异质相，而 Mo 作为强形成硼化物元素，会使 B 出现富集。

1 250～1 230 ℃双温焊接工艺，高温阶段保温时间短，B, Si 元素的扩散距离较短，形成的瞬时液相宽度较小，母材向液相中间层溶解量小。降低温

度继续保温时，合金元素的扩散能力降低，由于 B 元素的扩散速度远远高于 Si 元素，因此 Si 元素未有足够的时间进行均匀化扩散，最终在焊缝区出现“馒头”峰变化。

20 钢管的 TLP 连接中，接头中未发现 CO_2 气孔[5]，而在 45MnMoB 中碳合金钢连接时却出现了 CO_2 气孔。这是由于 45MnMoB 的碳含量远远高于 20 钢，在开放的环境下进行焊接，其氧化趋势大大提高，焊接过程中就会形成大量的 CO_2 存在于液态中间层内。随着等温凝固和均匀化的进行，产生的 CO_2 气体一部分受焊接压力的作用被排除接头外，一部分气体会残留在接头内形成气孔和空洞，影响接头性能。研究表明[9]，加压可改善润湿性，同时减少界面空洞数量与空洞体积。考虑到地质钻杆对接头区的尺寸有技术要求，不能单纯的增大压力来消除空洞。因此如何设计施压形式，消除 45MnMoB 接头区空洞，有待进一步的研究。

4 结 论

（1）采用瞬时液相扩散连接技术可以完成 45MnMoB 地质钻杆的焊接，接头成形好，无摩擦焊的飞边和等离子焊的焊瘤，性能达到钻杆焊接接头技术要求，并且超过了 PAW－TIG 联焊接头性能。

（2）两种焊接工艺均可获得和母材相同的组织，但是双温焊接工艺可以减少异质相，提高接头的焊合率。

参考文献：

[1] 周大中，赵忠诚，孙忠民，等. 绳索取芯钻杆的等离子弧焊—钨极氩弧焊焊接[J]. 焊接，1996(3)：5－9.

[2] Duvall D S, Owczarski W A, Paulonis D F. TLP Bonding: a new method for joining heat resistant alloys[J]. Welding Journal, 1974, 53(4)：203－214.

[3] 陈思杰，井晓天，李辛庚. 瞬时液相扩散连接的双温工艺模型[J]. 焊接学报，2005，26(4)：69－72.

[4] 李辛庚，吴 军，严 黔，等. 瞬时液相扩散焊铁基非晶中间层合金：中国，ZL02135336.0[P]. 2005－03－02.

[5] 王学刚，严 黔，李辛庚. 20 钢管高温钎焊与瞬时液相扩散焊接组织与性能[J]. 焊接学报，2005，26(5)：56－60.

[6] 王学刚，严 黔，李辛庚. 5A02 铝合金的瞬时液相扩散连接技术研究[J]. 轻合金加工技术，2005，33(7)：41－43.

[7] Shirzadi A A, Wallach E R. Analytical modeling of transient liquid phase diffusion bonding when a temperature gradient is imposed[J]. Acta Materialia, 1999, 47(13)：3551－3560.

[8] 虞觉奇，易文质，陈邦迪，等. 二元合金状态图集[M]. 上海：上海科学技术出版社，1987.

[9] 邹贵生，吴爱萍，任家烈，等. 连接压力在 Ti/Ni/Ti 复合层 TLP 扩散连接 Si3N4 陶瓷中的作用机制[J]. 宇航材料工艺，2000(4)：76－80.

作者简介：王学刚，男，1975 年出生，工学硕士，工程师。研究方向为非晶中间层开发和液相扩散连接工艺研究，获国家专利 4 项，省级科技进步一等奖 1 项，发表论文 10 篇。

Email：wxuegang@sohu.com

on the pin is clockwise, the metal around the pin will move upwards to the root of the pin and moves outwards along the shoulder surface, which causes that the center of the nugget will located at the upper part of the weld section. By using the pin with cylindrical shape, the transverse weld section appears onion ring pattern; but the onion ring pattern is not clear in the weld transverse section for the pin with taper shape or cam shape. If the length of the pin and shape at the tip are changed, the flow state of the plasticized metal below the pin and around the tip of the pin will be changed, therefore, the morphology of the weld at the bottom will change and the depth that the aluminum layer on the back surface of the plate enteed into the weld will be larger.

Key words: friction stir welding; pin shape; plastic flow; transverse weld morphology

Extraction of diagnostic information of expulsion defect in resistance spot welding process by wavelet analysis method XUE Haitao, LI Yongyan, CUI Chunxiang, DONG Tianshun (School of Material Science and Engineering, Hebei University of Technology, Tianjin 300132, China). p38—40

Abstract: An effective approach was developed to extract diagnostic information used to identify expulsion from electrode force curve by using wavelets analysis method for aluminum alloy shock wave resistance spot welding. The irregular signal singularity of electrode force curve was detected by using db5 wavelet. The detection result shows that the location and intensity of the signal singularity can be detected accurately from high frequency reconstructed signal of wavelet decomposition structure. That is to say, the expulsion can be identified easily. The diagnostic information is the global maximum value of high frequency reconstructed signal. The recognition method is that if the global maximum value exceeds the threshold value built by analyzing a number of testing data, the expulsion will occur. The testing result proves that the method is correct, reliable and credible. Therefore, the signal characteristic of electrode fore curve can be transformed into numerical characteristic that can be identified by computer.

Key words: aluminum alloy resistance spot welding; expulsion; wavelet analysis; diagnostic information

Effect of TiB_2 on microstructure and properties of Ni-based alloy coating by laser cladding YUAN Xiaomin, GONG Youpin, HE Yizhu (Anhui Key Laboratory of Materials and Processing, Anhui University of Technology, Maanshan 243002, Anhui, China). p41—44

Abstract: Ni-base alloy and TiB_2/Ni-based alloy metal-ceramics coatings were obtained on low carbon steel surface by 5 kW CO_2 laser. Microstructure, phases, microhardness and sliding wear resistance of the coatings were studied. The results shown that Ni-based alloy coating consists of γ-(Ni, Fe), $Cr_{23}C_6$ etc and TiB_2/Ni-based alloy composite coating consists of γ-(Ni, Fe), Ni_3B, TiB_2 and TiC and so on. The Ni-based alloy coating is made up of flourishing γ-(Ni, Fe) dendrite and eutectic structure. Equiaxed solid solution and fine eutectic structure are observed in the TiB_2/Ni-based alloy composite coating. The influence of TiB_2 ceramics on microstructure of coating is prominent that the microstructure of coating is finer and the dendrite crystal gradually becomes equiaxed grain. The microhardness and wear resistance of Ni-based alloy can be improved remarkablely by adding TiB_2.

Key words: laser cladding; Ni-based alloy; TiB_2; metal-ceramics layers; microstructure

Effect of magetic field parameters on microstructure and properties of welded joint of AZ31 magnesium alloy SU Yunhai[1], LIU Zhengjun[1], WANG Yu[2], ZHANG Guiqing[1] (1. Department of Material Sciences and Engineering, Shenyang University of Technology, Shenyang 110023, China; 2. Shenyang Special Type Equipment Examining Academe, Shenyang 110035, China). p45—48

Abstract: AC lognitudinal magnetic field was employed in welding of 5 mm thick AZ31 magnesium alloy plate with GTAW. The effect of magnetic field parameters on properties and microstructure of welded joint of AZ31 was studied through analysing the tensile strength, hardness and microstruture. The action mechanism of magnetic field was explored. The results indicated that the molten pool is stirred by the AC lognitudinal magnetic field, the solidification process is changed, the crystal grain is refined, and tensile strength and hardness of welded joint are improved. The molten pool is purified by the eletromagnetic stirring, so the gas pore and sensitivity of hot crack are decreased, and the formation of hot crack was supressed.

Key words: alternating current longitudinal magnetic field; AZ31magnesium alloy; gas tungsten arc welding; mechanical property

Numerical simulation of temperature field on complicated parts during plasma deposition dieless manufacturing WANG Guilan[1], WU Shengchuan[2], ZHANG Haiou[2] (1. College of Material Science and Engineering, Huazhong University of Science and Technology, Wuhan 430074, China; 2. State Key Laboratory of Digital Manufacturing Equipment and Technology, Huazhong University of Science and Technology, Wuhan 430074, China). p49—52

Abstract: A hybrid Gauss-double-Ellipse heat source model and a radiation-convection model were introduced to simulate plasma arc heat source and thermal boundary conditions. To improve the computational efficiency and reproduce the forming process, element Death & Birth and adaptive mesh techniques were used especially. Moreover, APDL code was developed to optimize fabrication process of a complicated part by plasma deposition dieless manufacturing, and some experiments were also conducted. Numerical and experimental results show that symmetrical jump-scanned paths together with suitable heat input and cooling approaches are effectively to improve the temperature distribution of parts and free contractility of weld, and thus lower stress level and hot crackability can be obtained, which eventually improve the possibly-intended formability.

Key words: plasma deposition dieless manufacturing; temperature field; finite element analysis; symmetrical jump-scanned paths; hot crackability

Transient liquid phase bonding of 45MnMoB steel geological

drill pipe using two-step heating process WANG Xuegang, YAN Qian, LI Xingeng (Laboratory of Special Welding and New Materials, Shandong Electric Power College, Jinan 250002, China). p53—56

Abstract: The geological drill pipe (45MnMoB steel) was joined by transient liquid phase bonding with a novel two-step heating process. The mechanical properties and microstructures of the joint were investigated, and compared with those of the joint produced by the conventional heating process. The results showed that both the heating processes produced a homogenous joint with microstructure and composition equivalent to the base metal. Compared with the conventional one-step heating process, the two-step heating process (1 250 ℃, 1 min and 1 230 ℃, 2 min) remove the dissimilar interfaces, and increased the bonded ratio, and get the joint with tensile strength of 890 MPa and bending degree of 180°, which exceeded the technical criterions of geological drill pipe. As this technology can be applied in drill pipe production without postweld machining process, and the production costs will be reduced.

Key words: geological drill pipe; 45MnMoB steel; transient liquid phase bonding; two-step heating; mechanical properties

Effect of postweld heat treatment on microstructure of electron beam welded joints of Ti_3Al HE Jingshan, ZHANG Binggang, WU Qingsheng, LIU Wei (State Key Laboratory of Advanced Welding Production Technology, Harbin Institute of Technology, Harbin 150001, China). p57—60

Abstract: The postweld heat treatment of the electron beam welded joints of Ti_3Al—Nb was carried out at 650 ℃ and 1 000 ℃ for 2 hours, respectively. Its effect on the microstructure of electron beam welded joints of Ti_3Al was investigated. Experimental results show that the microstructure of the weld under welding conditions is predominantly metastable, the columnar crystal metastructure of $B2$ phase. The microstructure of the weld is significantly influenced by the method of the heat treatment. The microstructure of the weld for postweld heat treatment at 1 000 ℃ for 2 hours is the laminar structure (Widmanstaten structure) consisted of interphase α_2 and $B2$. After postweld heat treatment at 650 ℃ for 2 hours, the small α_2 phase is precipitated in grain boundary and intragranular of $B2$ phase in the weld. After postweld heat treatment, whether 650 ℃/2 h or 1 000 ℃/2 h, the microhardness distribution of the joints are both more uniform than that of the weld without heat treatment. However, The whole joint is softened after the postweld heat treatment at 1 000 ℃ for 2 hours and the microhardness of the whole joint is not higher than that of postweld heat treatment at 650 ℃ for 2 hours.

Key words: Ti_3Al; electron beam welding; postweld heat treatment; microstructure

Thermodynamic analysis on intermediate transformation mechanism of acicular ferrite in welds XU Xiaofeng, LEI Yi (College of Mechanical and Electronic Engineering, China University of Petroleum, Dongying 257061, Shandong, China). p61—64

Abstract: Based on the fact that carbon-depleted regions come into being during the incubation period, thermodynamic models of diffusion and shear for weld acicular ferrite (AF) transformation in carbon-depleted regions of austenite were established respectively by using KRC (Kaufman, Radcliffe, Cohen) activity model and super-element algorithm, and used in the numerical simulation of a certain microalloy steel. The results show that with the variation of carbon content in the carbon-depleted region, the transformation mechanism of AF is different. The driving force in diffusion model is greater than that of shear model when the carbon content is much higher, while the driving force in shear model is a little greater than that of diffusion model when the carbon content is much lower. If there is no carbon in the carbon-depleted region, the driving forces of both models will be equal. The driving forces of the two models show the similar tendency, and increase with the decreasing of carbon content in carbon-depleted regions and AF transformation temperature.

Key words: acicular ferrite; carbon-depleted region; diffusion; shear; thermodynamics

Lap seam welding of magnesium alloy with variable polarity plasma arc JIANG Jianbo, LIU Liming, ZHU Meili, SHEN Yong (State Key Laboratory of Materials Modification, Dalian University of Technology, Dalian 116024, Liaoning, China). p65—68

Abstract: The keyhole variable polarity plasma welding was used to weld AZ31B Mg alloy, and favorable joint was obtained. The microstructure, mechanical properties and hardness were investigated by the optical microscope, tensile testing machine and hardness instrument. The results show that one side welding with back formation can be obtained through this technique when there is no groove and no enclosed protection; the heat-affected zone is narrow, and the average tensile shear is 7.3 kN; the grains of fusion zone are fine, and the hardness of welded joint is higher than that of the base metal. In summary, the variable polarity plasma arc welding process is a perfect method to weld Mg alloy, which can improve the microstructure of the joint and increase the welding quality.

Key words: keyhole variable polarity plasma welding; lap seam welding; magnesium alloy; microstructure

Ultrasonic evaluation of interface quality of TiAl and 40Cr diffusion welding LUAN Yilin, GANG Tie (State Key Laboratory of Advanced Welding Production Technology, Harbin Institute of Technology, Harbin 150001, China). p69—72

Abstract: The quality of TiAl and 40Cr diffusion welding interface was inspected by ultrasonic C-scan method and the relationships between mean and standard deviation of amplitude of interface echo and shear strength were studied. The effects of weld temperatures and surface roughnesses of specimens on above-mentioned relationships were investigated and the relationship between the amplitude and length of air gap was discussed. It is found that at a given surface roughness, bonding strength increases with the decreasing of mean and standard deviation of amplitude. The relationships between mean and standard deviation of amplitude of interface echo and shear strength are influenced by surface roughness. When the length of air gap is shorter than 400 μm, the amplitude of interface echo is approximately in proportion to the length of air gap.

Key words: ultrasonic test; C-scan; diffusion welding; dis-